Available online at www.sciencedirect.com
SCIENCE DIRECT
Polymer 46 (2005) 11569–11581
polymer
www.elsevier.com/locate/polymer

Polystyrenes with macro-intercalated organoclay. Part II. Rheology and mechanical performance

Maryam Sepehr [a], Leszek A. Utracki [a,*], Xiaoxia Zheng [b], Charles A. Wilkie [b]

[a] *Industrial Materials Institute, National Research Council Canada, 75 de Mortagne, Boucherville, Que., Canada J4B 6Y4*
[b] *Department of Chemistry, Marquette University, P.O. Box 1881, Milwaukee, WI 53201, USA*

Received 23 August 2005; received in revised form 5 October 2005; accepted 5 October 2005
Available online 27 October 2005

Abstract

Polymeric nanocomposites (PNC) of polstyrene (PS) with organoclay were studied for their rheological and mechanical behavior. The organoclay (COPS) is a product of clay quaternization with a copolymer of styrene with vinyl benzyl tri-methyl ammonium chloride. PNC preparation and characterization was described in Part I of this paper. The clay platelets in COPS and its PNC's are well dispersed, i.e. with the interlayer spacings of $d_{001}=7$–8 nm. By contrast, $d_{001}=3$–4 nm for PNC with Cloisite® 10A. However, the COPS in PS formed large, deformable domains. At concentration exceeding 5.8-wt% of COPS, the domains started to form a three-dimensional network with enhanced elasticity and progressive viscoelastic non-linearity. At temperatures of 160–180 °C the neat COPS did not flow; its behavior resembled that of a crosslinked elastomer. Application of the time–temperature superposition led to master curves of bending moduli vs. 19 decades of reduced frequency. The curves indicated a transition at ca. 180 °C, most likely associated with the disintegration of ammonium ion clusters. With the same amount of clay the mechanical properties of PNC with COPS were slightly worse than those with Cloisite® 10A—the immiscibility of COPS, and the presence of extractable (by the matrix) low molecular weight compounds explain the behavior.

Keywords: Polystyrene; Nanocomposites; Phase separation

1. Introduction

To optimize performance of a polymer/clay nanocomposite (PNC) the individual clay platelets should be randomly dispersed in a polymeric matrix; hence exfoliated. For this purpose usually clay is intercalated, and then either dispersed in a monomer, which subsequently is polymerized (reactive exfoliation), or mechanically dispersed in a molten polymer, with or without a compatibilizer (mechanical exfoliation) [1]. For several strategic and economic reasons the latter method is advantageous [2]. However, for the mechanical exfoliation to be successful the PNC must be homogenous, thus miscible. It is the thermodynamics that determines whether PNC can be exfoliated or not—the compounding/mixing/dispersion process may only accelerate the exfoliation. In most systems the intercalant/matrix immiscibility prevents the exfoliation.

Exfoliation of clay platelets in a nonpolar polymer such as polystyrene (PS) or polypropylene (PP) is particularly difficult. Compounding of commercial organoclays with PS invariably results in aggregation of intercalated clay stacks [3–9]. Although intercalation of PS or PP matrix between clay platelets has been observed, exfoliation was not. During the melt compounding the stress and strain controlled dispersion of organoclay is accompanied by the thermal degradation of the ammonium intercalant, which follows the Hofmann elimination reaction [7–10]. The latter process starts at about 150 °C [1,11].

The mathematical modeling of clay dispersion (based on the equilibrium thermodynamics) indicates that the most effective intercalant should be macromolecular in nature, miscible with the matrix polymer, and having reactive end group capable of bonding to the clay surface [12,13]. In principle, there are two ways to prepare organoclay intercalated with end-terminated macromolecules: (1) by dispersing organoclay pre-intercalated with a vinyl-terminated reactive compound [14–17] in a monomer (e.g. styrene), and then co-polymerizing. (2) Preparing a polymer (e.g. PS) end terminated with, e.g. ammonium ion [18], and reacting it with clay.

More recently, Wilkie and his collaborators developed an alternative method of clay exfoliation in PS matrix [19–21]. The method involves free radical copolymerization of

* Corresponding author. Tel.: +1 450 641 5182; fax: +1 450 641 5105.
E-mail address: leszek.utracki@cnrc-nrc.gc.ca (L.A. Utracki).

0032-3861/$ - see front matter © 2005 Elsevier Ltd. All rights reserved.
doi:10.1016/j.polymer.2005.10.032

Table 1
Composition, XRD results, rheological and mechanical properties for the prepared samples

Identification code	Composition				XRD results		Rheological properties				Mechanical properties				
	Grade of PS	Organo-clay	Organo-clay (wt%)	Clay-MMT (wt%)	d_{001} (nm)	Number of platelets per stack	Equation used	η_0 (kPa s)	σ_y (kPa)	n (power law exponent)	Tensile strength (MPa)	Tensile modulus (GPa)	Flexural strength (MPa)	Flexural modulus (GPa)	Impact strength (J/m)
As received	1301	–	0	0	–	–	1	76.6	–	0.001	46.9	3.31	99.9	3.33	14
B1	1301	–	0	0	–	–	1	71.5	–	0.15	–	–	–	–	–
B4	1301	COPS	4.35	0.9	7.1	5.7	1	71.1	–	0.15	–	–	–	–	–
B5b	1301	COPS	8.7	1.9	6.9	12.5	1	66.8	–	0.07	–	–	–	–	–
B21	20.3	–	0	0	–	–	1, 2	32.2	(0.4 ± 0.6)	0.25	–	–	–	–	–
B23	20.3	COPS	12.5	2.7	7.9	2.5	1, 2	72.3	0.96 ± 0.1	0.27	–	–	–	–	–
B24	20.3	COPS	25	5.4	7.9	2.7	1, 2	160.3	4.2 ± 0.3	0.29	–	–	–	–	–
B25	20.3	COPS	49.8	10.8	8.0	4.1	1, 2	414.0	11.0 ± 1.3	0.23	–	–	–	–	–
PS1	1301	–	0	0	–	–	–	–	–	–	45.9	3.24	99.2	3.36	13
PS2	1301	COPS	5.2	1.1	6.5	7.0	–	–	–	–	40.7	3.48	62.1	3.61	8
PS3	1301	–	0	0	–	–	1	55.0	–	0.012	45.7	3.20	99.9	3.37	13
PS4	1301	COPS	5.2	1.1	6.4	6.4	1	45.7	–	0.007	41.5	3.46	64.7	3.58	9
PS5	1301	C10A	2	1.2	4.3	5.7	1	65	–	0.03	43.4	3.43	83.6	3.49	13
Error of measurements					±0.2	5%			±1.02		1.8%	3.6%	2.0%	1.1%	11%

Note: The identification codes of the samples in column 1 are used in the text. Samples coded B- were prepared in a mini-TSE-CoR; those coded PS1 and PS2 were compounded in TSE-34, while PS3, PS4, and PS5 in TSE + GP + EFM (C–D gap = 15 μm—see part I).

vinyl-benzyl trimethyl ammonium chloride (VBTACl) with styrene, followed by intercalation of sodium montmorillonite (Na-MMT). The process results in grafting each MMT platelet with ca. 45,000 copolymer molecules having the molecular weight of about 5 kg/mol—the material is identified in this text as COPS [22].

The original aim of this work was to examine whether COPS might be used to produce exfoliated PS-based PNC. Three criteria might be used to evaluate the organoclay performance: (1) degree of clay dispersion, (2) thermal stability during compounding and processing, and (3) the product performance.

As described in Part I [22], two methods were used for the preparation of PS-based PNC with COPS: melt compounding and co-solubilization. According to XRD, the clay platelets in COPS and its PNC with PS are relatively well dispersed, having large interlayer spacings of $d_{001}=7$–8 nm (that in PNC with commercial organoclay ranges from 3 to 4 nm). SEM and TEM confirmed the interlayer spacings but at the same time indicated phase separation. Apparently, the statistical nature of the styrene-VBTA copolymer results in a partially crosslinked COPS network structure. In this part, the flow behavior and mechanical properties will be examined.

2. Experimental

2.1. Materials

Two commercial polystyrenes: PS20.3 and PS1301 (having the weight-averaged molecular weight $M_w=116$ and 270 kg/mol, respectively), and two organoclays (Cloisite® 10A; C10A, and COPS) were used. PNC's comprising ca. 0.9–10.8-wt% of MMT were prepared by melt compounding. Compounding was carried out either in a co-rotating mini-TSE or using a compounding line of Leistritz TSE-34 ($L/D=40$) with gear-pump (GP) and the Extensional Flow Mixer, EFM (see Part I [22]). The prepared and tested samples are listed in Table 1.

2.2. Dispersion of COPS in PS

As detailed in Part I [22] COPS and its mixtures with PS were characterized by X-ray diffraction (XRD), transmission electron microscopy (TEM), scanning electron microscopy (SEM), and analyzed for volatiles using the thermo-gravimetric analyzer (TGA).

The XRD measurements yielded the interlayer spacing (d_{001}), and the thickness of the diffracting clay stack, t. From these two, the number of clay platelets per average stack was calculated as: $m=1+t/d_{001}$. The results for PNC's with COPS and for C10A (at the same MMT content) were quite different, e.g. $d_{001}=8.8$ and 1.94 nm, or $t=56$ and 7.5 nm, respectively. Characteristically, melt compounding PS with COPS or with C10A showed opposite tendencies—while the stack thickness increased for COPS, for C10A it decreased.

TEM confirmed the large interlayer spacing calculated from XRD for COPS and its mixtures. However, more interesting were the results from SEM, which for the COPS/PS mixtures indicated the presence of large (10–18 μm) aggregates. Their presence in samples prepared by co-dissolution indicated thermodynamic immiscibility.

2.3. Melt rheology

The dynamic rheological measurements were performed in an ARES rotational rheometer, using 25 mm diameter parallel plates in oscillatory shear mode under a blanket of dry nitrogen at $T=160$ and 180 °C. Prior to testing the specimens were dried for at least 48 h under vacuum at 80 °C. Three types of tests were carried out: (1) the time sweep at frequency $\omega=6.28$ rad/s, and strain $\gamma=0.05$ for time $t\geq 3600$ s; (2) the strain sweep at $\omega=1$ rad/s, for $\gamma=0.01$–1; (3) the frequency sweep at $\gamma=0.05$ within the frequency range from $\omega=0.01$ to 100 rad/s.

2.4. Dynamic mechanical thermal analysis (DMTA)

The measurements were performed in DMTA V analyzer (Rheometrics Scientific), using the single-cantilever-bending fixture. The specimens were compression molded at $T=160$ or 180 °C under pressure of $P=318$–1272 kPa for 4 min (always using the same test procedure and specimen dimensions $27\times 7\times 1.6$ mm^3). Three types of tests were carried out within the linear viscoelastic region: (1) the strain sweep at frequency $\omega=6.28$ rad/s from $\gamma=0.0001$–0.005; (2) the temperature sweep at $\omega=6.28$ rad/s, from $T=30$ to 140 or 160 or 170 °C, at the strain determined by the strain sweep, $\gamma=0.0004$; and (3) the frequency sweep at $\gamma=0.0004$, from $\omega=0.0628$ to 62.8 rad/s, at $T=30$–170 °C with the step of $\Delta T=10$ °C. In the latter test, to stabilize the temperature, a delay of 180 s was used.

2.5. Mechanical testing

Extruded PNC pellets were injection molded using Engel 150T machine into standard dogbone specimens for tensile tests (ASTM D638, type I), and rectangular specimens for flexural ones (ASTM D790). The bars for Izod impact tests (ASTM D256) were cut from the narrow section of dogbone specimens. The barrel temperature was 200 °C, injection pressure of 18 MPa, mold temperature of 40 °C, holding pressure of 7 MPa, and cooling time of 20 s.

Tensile tests were carried out according to ASTM D638 using an Instron 5500R model 1125 tester. Crosshead speed was 5 mm/min. An extensometer was used to accurately measure the strain. Young's modulus was calculated by least square polynomial fitting of the experimental data of stress versus strain in the initial region of strain from 0 to 0.2%. Flexural tests (ASTM D790) were carried out using the same tester. The rate of crosshead motion was set up at 15.7 mm/min and the dimension of support span was 59 mm.

Notched Izod impact tests (ASTM D256) were performed at room temperature using an Instron Model 8200 impact tester.

The reported values are averages of 10 tests for each composition.

3. Results

3.1. Rheology of PS/COPS

The rheological behavior of three families of PS/COPS compounds was studied: (1) PS1301 without and with COPS (batches B1, B4 and B5b prepared in mini-TSE); (2) PS20.3 without and with COPS (stabilized with 0.5-wt% of Irganox B215, viz. batches B21 and B23–B25 prepared in mini-TSE); (3) PS1301 without and with 1.2-wt% MMT (batches PS3–PS5 prepared in TSE + GP + EFM).

The three types of dynamic tests (see part 3.4) were carried out:

1. The time sweep at $T = 160$ and 180 °C for PS20.3, and PS1301 or their PNC, respectively.
2. The strain sweeps, at the same temperatures, and frequency of $\omega = 1$ rad/s.
3. The frequency sweep within the linear viscoelastic range at low strain of $\gamma_0 = 0.05$ and frequency range of, $\omega = 0.01$ to 100 rad/s (Figs. 3 – 6).

3.1.1. Time sweep

The time sweep results are presented in Figs. 1 and 2, as dynamic moduli (storage, G', and loss, G'') vs. test time. Fig. 1 shows the behavior of neat PS20.3 and PS1301 at $T = 160$ and 180 °C, respectively. It is noteworthy that the former polymer remained stable for more than 2 h, but PS1301 at $T = 180$ °C initially ($t < 2000$ s) increased by about 4.4%, and then stabilized for at least 1 h. This difference of behavior may be due to the temperature difference, which accelerates loss of residual styrene.

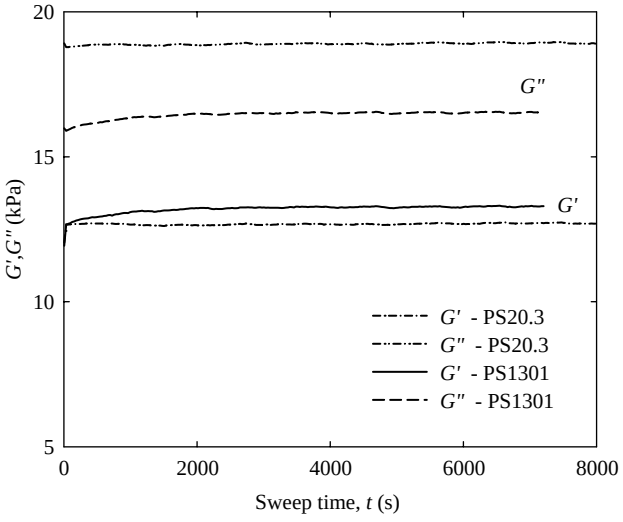

Fig. 1. Storage and loss moduli vs. sweep time for PS20.3 at $T = 160$ °C, and PS1301 at $T = 180$ °C ($\omega = 0.628$ rad/s and $\gamma_0 = 0.05$).

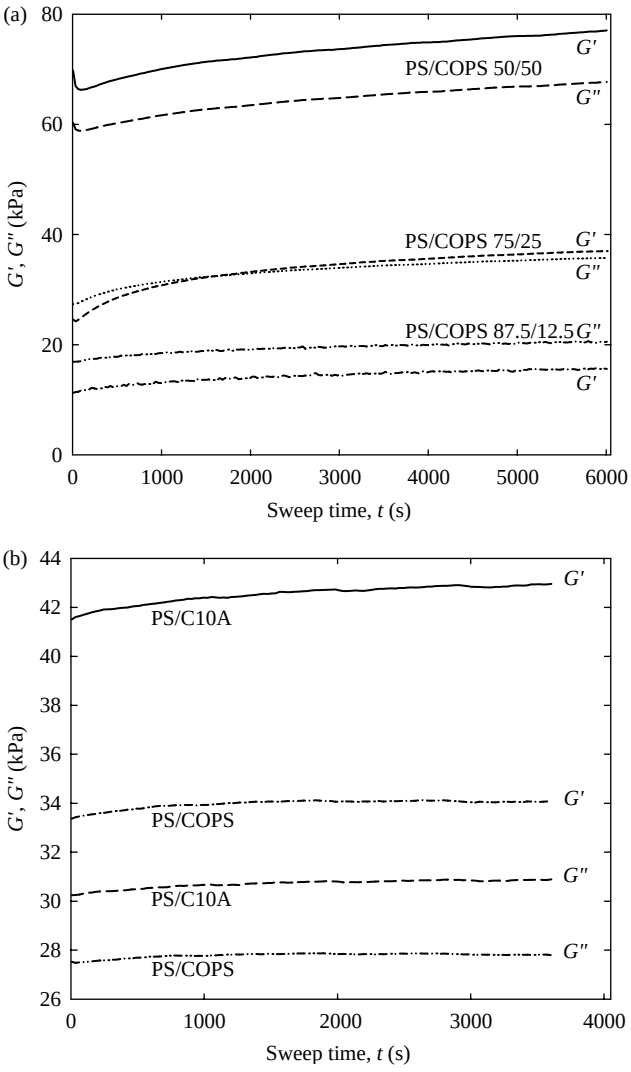

Fig. 2. Storage and loss moduli recorded during time sweep at strain of $\gamma_0 = 0.05$ for (a) PS20.3/COPS at $T = 160$ °C and $\omega = 0.628$ rad/s; (b) PS1301/organoclay prepared in TSE + GP + EFM at $T = 180$ °C, and $\omega = 6.28$ rad/s.

The time sweeps of PS20.3 with 12.5–50-wt% of COPS (B23 to B25; see Table 1) are presented in Fig. 2(a) and those of PS1301 with organoclays (PS4 and PS5) in Fig. 2(b). As is evident from the data in Table 1, the inorganic clay content is similar for the latter two systems, but the dynamic shear moduli of PNC with C10A are significantly higher. During the time sweep G' and G'' of samples B23 to B25 increase by 2–25% in the first 1000 s, then by an additional 10–25% during the next 5000 s. By contrast, the moduli of compounds PS4 and PS5 increased by 1—3.5% during 1 h of testing. The increase of the rheological signals depends on the amount of COPS in the specimen, and is caused by evaporation of volatiles—judging by the characteristic smell, mainly by loss of styrene (boiling point 146 °C).

3.1.2. Strain sweep

Fig. 3 shows the storage and loss moduli as functions of shear strain, $\gamma = 0.01$–1, at frequency of $\omega = 1$ rad/s, for two PS resins. The moduli are constant up to critical strain value, γ_c,

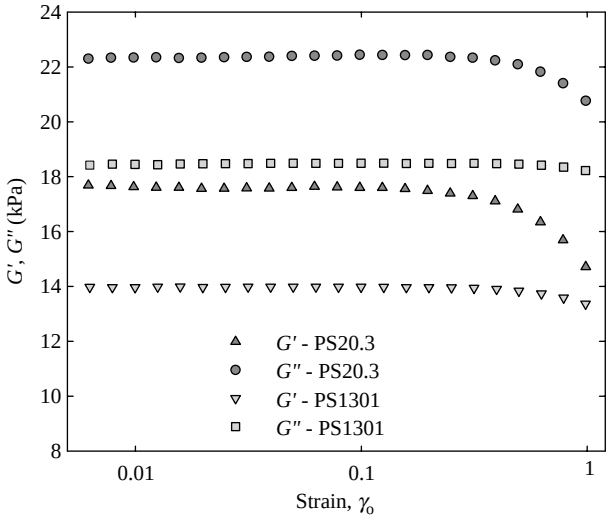

Fig. 3. Storage and loss shear moduli vs. sweep strain for PS1301 at $T=180$ °C and PS20.3 at $T=160$ °C and $\omega=1$ rad/s.

and then decrease. Results indicate that the linear viscoelastic region of PS20.3 and PS1301 extends to $\gamma_c \cong 0.16$ and 0.30, respectively. The strain sweep of PS1301 at $\omega=0.1$ and 10 rad/s, gave $\gamma_c \cong 0.60$ and 0.20, respectively. The increase of frequency reduces γ_c, viz. $\gamma_c \cong 0.330/\omega^{0.239}$. The strain sweeps of B4, B5b and B23 gave $\gamma_c \cong 0.15$, 0.12 and 0.10, respectively. In all the subsequent time and frequency sweeps, the shear strain was kept constant at $\gamma=0.05$.

3.1.3. Frequency sweep

Examples of results obtained during the frequency sweeps are displayed in Figs. 4 and 5, respectively for samples containing a low concentration of organoclay, and for those with high concentration.

The results presented in Fig. 4 correspond to the frequency sweep for samples containing 1.2-wt% MMT (samples PS3 to PS5 in Table 1). The tests were carried out at $T=180$ °C and $\gamma_0=0.05$ and the scanning started at the highest frequency, $\omega=100$ rad/s. Fig. 4(b) represents the experimental results of dynamic viscosity vs. frequency and also the computed one from Eq. (1).

The results of the frequency sweeps for samples containing larger amounts of COPS are presented in Fig. 5. The tests were conducted at $T=160$ °C and $\gamma_0=0.05$ for PS20.3 with 0, 12.5, 25, and 50-wt% COPS (samples B21 and B23 to B25 in Table 1). The scanning was conducted starting at the highest frequency, $\omega=100$, and decreasing it to $\omega=0.01$ rad/s. The figure displays the storage and loss moduli vs. frequency. It is noteworthy that the crossover frequency at which the two moduli are equal, $\omega_x=\omega|_{(G'=G'')}$, as well as the initial slopes of the moduli at frequencies $\omega<0.1$ rad/s, $\mathrm{dln}\, G'/\mathrm{dln}\,\omega$ and $\mathrm{dln}\, G''/\mathrm{dln}\,\omega$, all depend on COPS content.

Another representation of the rheological behavior of PNC's containing large amount of COPS is presented in Fig. 6. Here the coefficients of moduli, defined as $\eta''=G'/\omega$ and $\eta'=G''/\omega$, are plotted vs. ω. Fig. 6(a) and (b) represents, respectively, the loss and dynamic viscosities vs. frequency. In Fig. 6(b), the

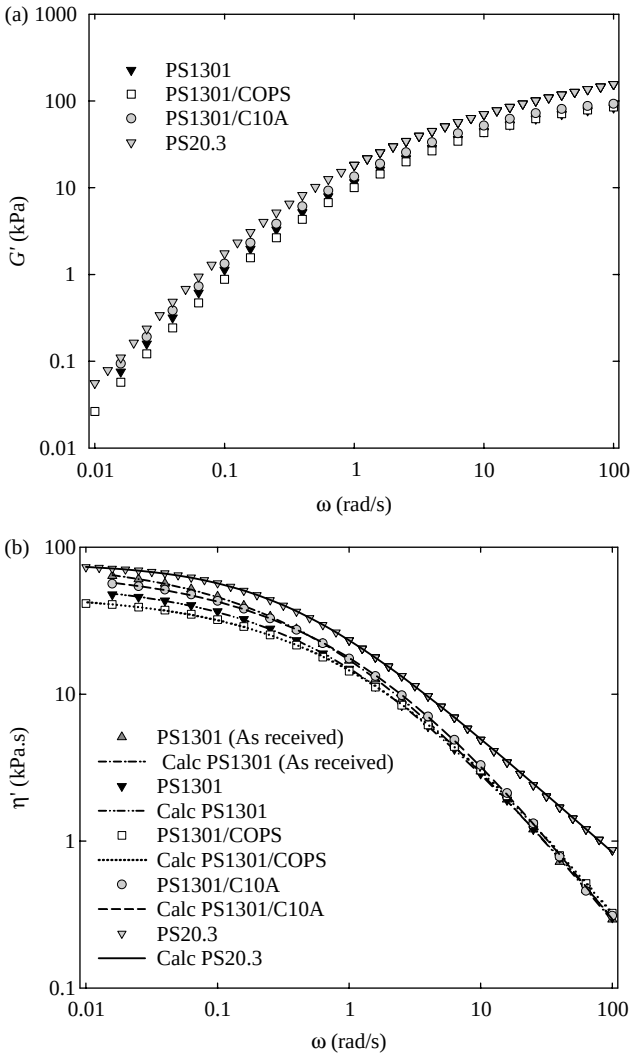

Fig. 4. Frequency sweeps at $\gamma_0=0.05$ for PS20.3 at $T=160$ °C,as well as for PS1301 and its mixtures containing ca. 1.2-wt% MMT at $T=180$ °C (samples PS3 to PS5). (a) The storage modulus vs. frequency, and (b) the dynamic viscosity vs. frequency.

points are experimental while the lines are computed from Eqs. (1) to (2) (Section 4).

The data of Figs. 4 and 5 are replotted in Fig. 7(a) and (b) as G'/G'' vs. G''. It is noteworthy that the correlation between G' and G'' at low frequency is similar not only for the two homopolymers, but also for the PNC's containing ca. 1.2 wt% MMT (samples PS4 and PS5 in Table 1) as well. The results show a dramatic change in rheological behavior when the COPS content increases from 5.2 (Fig. 7(a)) to 12.5-wt%, which corresponds to changes in MMT content from 1.13 to 2.71-wt%.

3.1.4. DMTA of PS/COPS compounds

For the DMTA tests, compression molded COPS specimens were prepared from mixtures of PS20.3 with 0, 12.5, 25, 50, and 100-wt% of COPS.

The tests were carried out within the linear viscoelastic region at low strains ($\gamma=0.0001$–0.005). The results of T-sweep at heating rate of 1 °C/min, and $\omega=6.28$ rad/s are

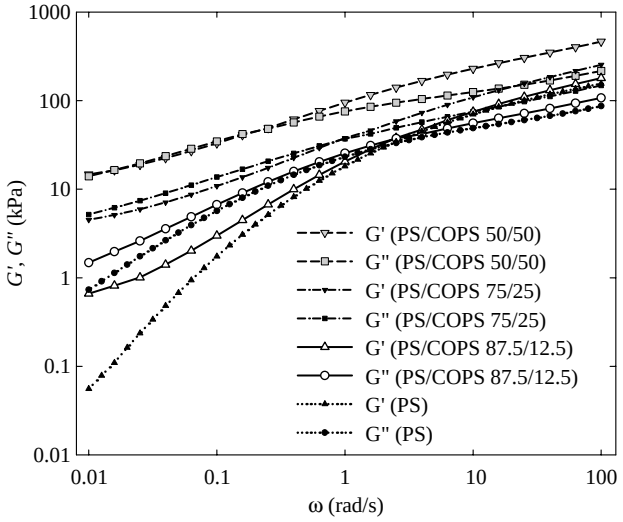

Fig. 5. The frequency dependence of the storage and loss moduli at $T=160\,^{\circ}C$ and $\gamma_0=0.05$ for PS20.3 with 0, 12.5, 25, and 50-wt% COPS (B21 and B23 to B25). The scan was carried out starting at $\omega=100$ rad/s.

presented in Fig. 8. Fig. 9 displays the results of low strain frequency sweeps, from $\omega=0.0628$ to 62.8 rad/s, at $T=30$–170 °C, with the step of $\Delta T=10\,^{\circ}C$. Using the time–temperature (t–T) superposition the master curves covering 19 decades of frequency were obtained.

3.2. Mechanical performance of PS/COPS compounds

The tensile tests were carried out following the ASTM D638-02a with specimens type I. The flexural tests followed ASTM D790-03, while the Izod impact tests that of ASTM D256-02 with notched specimens. The results are presented in Figs. 10–12, and summarized in Table 1.

4. Discussion

The main objective of the project was to prepare exfoliated PNC with PS as the matrix. For this purpose, COPS organoclay with macromolecular intercalant was prepared. The preparation involved two steps: the free radical copolymerization of styrene with vinyl-ammonium compound, followed by Na-MMT intercalation.

In Part I of this paper [22] the preparation and characterization of the corresponding PNC was presented. The clay platelets in COPS and its PNC with PS, having $d_{001}=$ 7–8 nm, were relatively well dispersed. By contrast, d_{001} in PNC with Cloisite® 10A was only 3–4 nm. However, the number of clay platelets per stack in PS/COPS was large: $m=$ 3–12, in comparison to $m=2$–6 determined for PS/C10A. Also, the scanning and transmission electron microscopy (SEM and TEM) indicated that in PS matrix COPS existed in form of large, immiscible domains. Thus, melt compounding of COPS with PS, instead of exfoliation, resulted in two-phase dispersions. The immiscibility between linear PS and COPS was also evident in samples prepared by the co-solvent method.

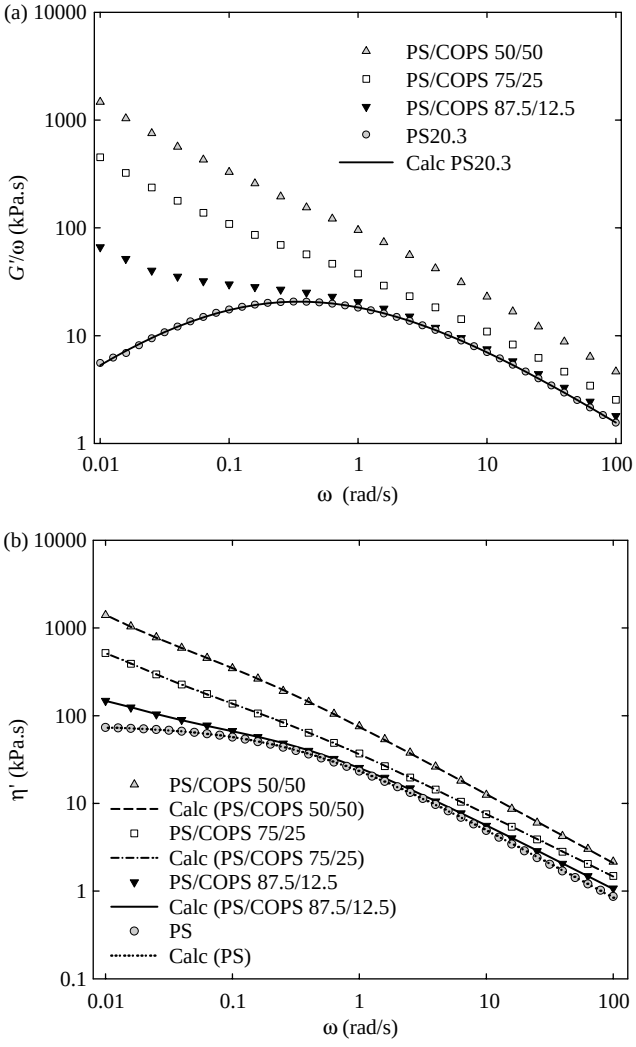

Fig. 6. Frequency dependence of (a) coefficient the storage modulus and (b) the dynamic viscosity at $T=160\,^{\circ}C$ and $\gamma_0=0.05$ for PS20.3 with 0, 12.5, 25, and 50-wt% COPS (samples B21 and B23 to B25). Line computed from Eqs. (1) and (2).

To confirm the conclusions based on the analytical test methods (viz. XRD, SEM, TEM) extensive rheological tests were performed. Furthermore, since PNC are primarily used as structural materials, the mechanical performance of several PS-based PNC's was studied. On the preceding pages of this Part II these two sets of data were presented, now they will be discussed considering the available information.

4.1. Rheological studies

The time sweeps for PS and its PNC's with COPS indicated the presence of volatiles in the latter materials, which caused increases of G' and G'' during the rheological tests. Since the frequency scan of four decades, recording either 5 or 10 points per decade lasts respectively 1400 or 5555 s, the raw data had to be corrected for the evaporation of volatiles, extrapolating to zero-test time.

Results of the frequency sweeps for PS1301 with ca. 1.2-wt% MMT are shown in Fig. 4. Near superposition of data for

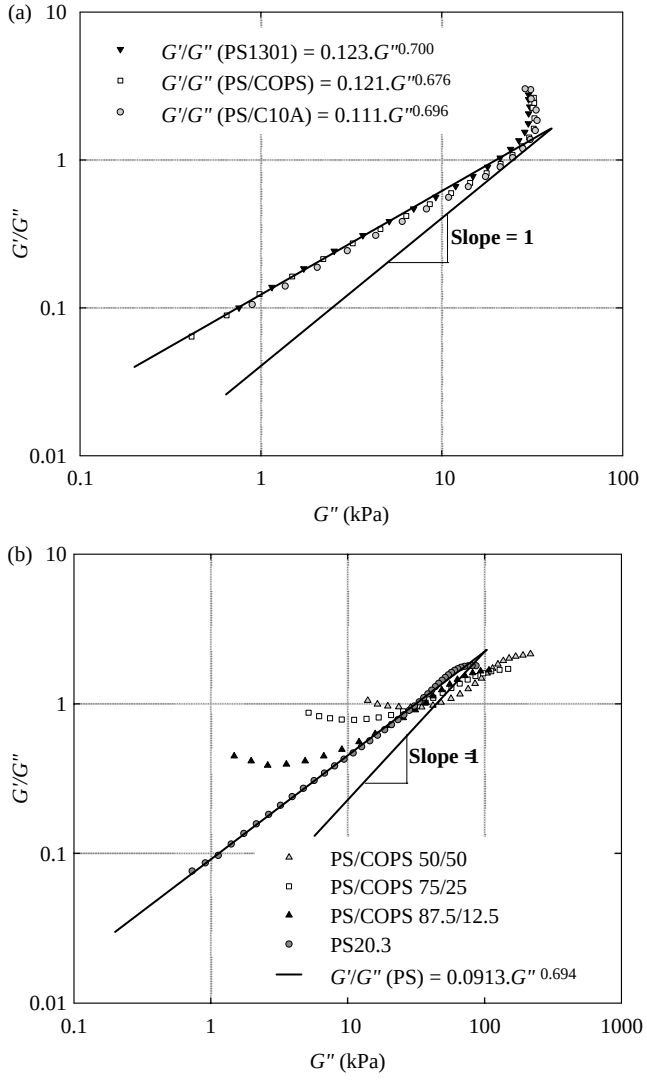

Fig. 7. The relation between the storage and loss moduli for (a) PS1301 and its mixtures containing ca. 1.2-wt% MMT (samples PS3 to PS5) at $T=180$ °C and $\gamma_0=0.05$; (b) PS20.3 with 0, 12.5, 25, and 50-wt% COPS (samples B21, B23 to B25) at $T=160$ °C and $\gamma_0=0.05$.

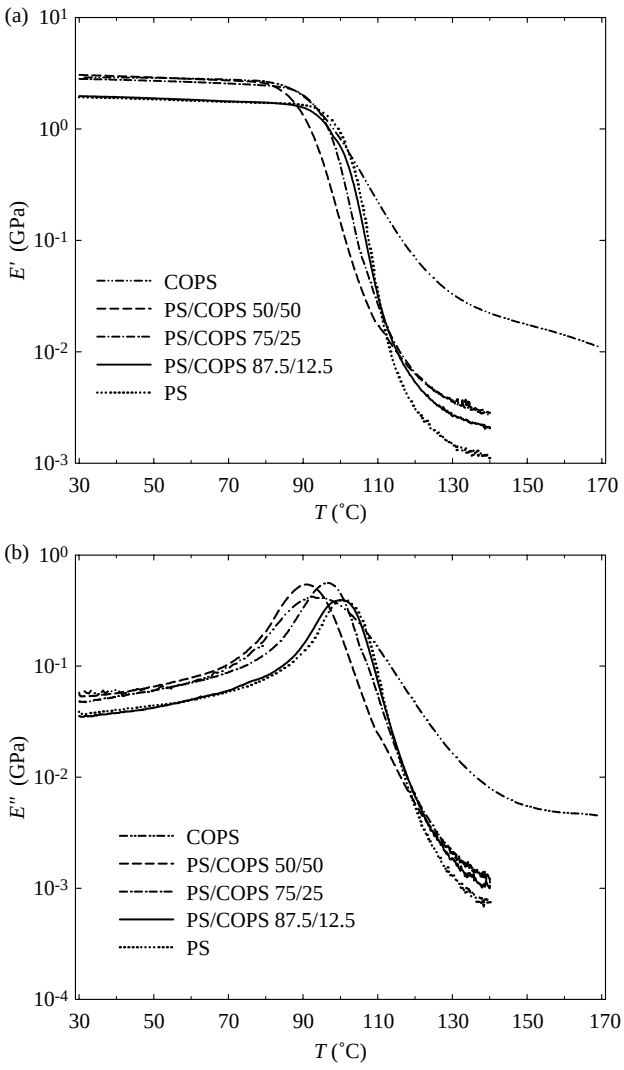

Fig. 8. Dynamic tensile moduli, the storage E' (a), and the loss E'' (b) for PS20.3 with 0, 12.5, 25, 50, and 100-wt% COPS vs. T at $\gamma=0.0004$, $\omega=6.28$ rad/s, and the heating rate of 1 °C/min.

the three PS1301 systems (PS3 to PS5) indicates that the melt structure is not affected by the presence of organoclay. The absence of the dynamic modulus, G', plateau at low frequencies confirm the results of XRD and TEM, the organoclay is not exfoliated in these compounds. The generalized Carreau–Yasuda equation (valid within the linear viscoelastic region) may be applied:

$$\eta' = \eta_0[1 + (\tau\omega)^a]^{(n-1)/a} \quad (1)$$

where η_0 is the zero shear viscosity, τ the relaxation time, n the power-law exponent and a is a parameter. As shown in Fig. 4(b), Eq. (1) describes the dependence well—the statistical fitting parameters and those of Eq. (1) are listed in Table 2. It is noteworthy that extrusion of PS1301 in a TSE+GP+EFM resulted in about 10% reduction of the polymer molecular weight.

Significantly, incorporation of 2-wt% C10A into PS1301 increased the zero-shear viscosity by ca. 20%, whereas incorporation of 5.2-wt% COPS (which contains about the same amount of MMT) reduced it by ca. 18%. The reduction most likely is caused by the presence of extractable oligomers. At $T=160$ °C the dynamic viscosity of PS20.3 is slightly higher than that of PS1301 at $T=180$ °C. The higher power-law index of PS20.3 indicates greater molecular polydispersity.

Another illustration of the same behavior is presented in Fig. 6, where the coefficients of moduli, here defined as G'/ω and $\eta'=G''/\omega$, are plotted vs. ω. The usual way of presenting the dynamic elasticity coefficient is as $\psi=G'/\omega^2$. The plot of ψ vs. ω resembles that of η' vs. ω (presented in Fig. 6(b)), and may be described by Eq. (1). On the other hand, plot of $G'/\omega=\psi\omega$ vs. ω makes the structural changes of the melt more evident. Both plots in Fig. 6 suggest the presence of tri-dimensional structures at higher COPS concentrations. Evidently, the immiscible domains of COPS start to interact at concentration somewhere between 8.9 (no interactions) and 12.5 (interactions present). To define this critical overlap concentration, ω_c, several rheological functions might be used.

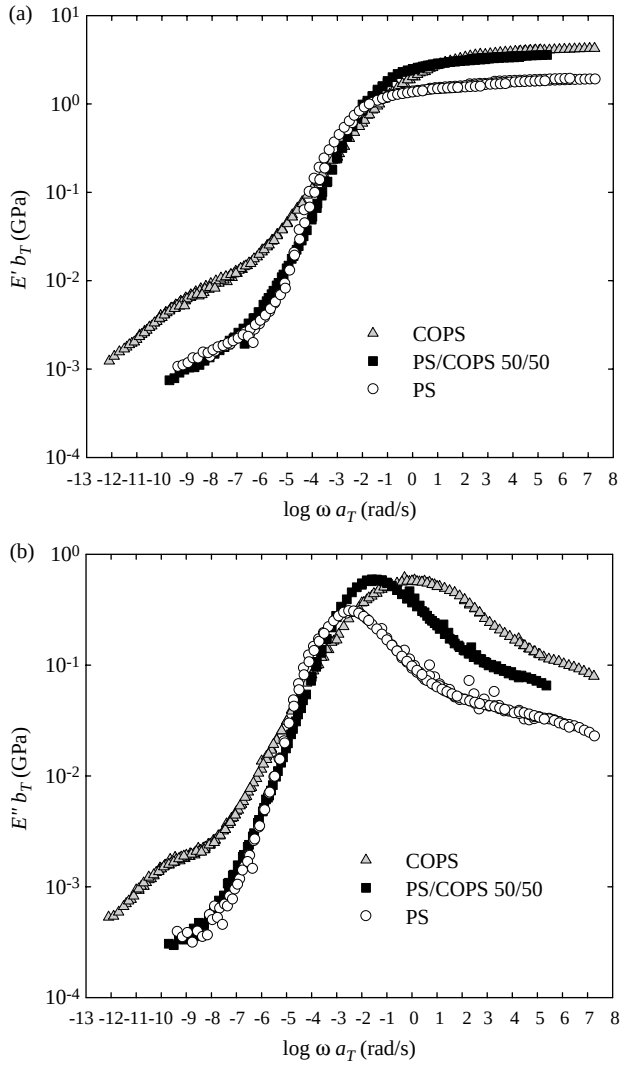

Fig. 9. The master curves of the storage and loss moduli for PS20.3 with 0, 50, and 100-wt% COPS as function of reduced frequency, ωa_T, at $\gamma = 0.0004$, and $T = 30$–170 °C.

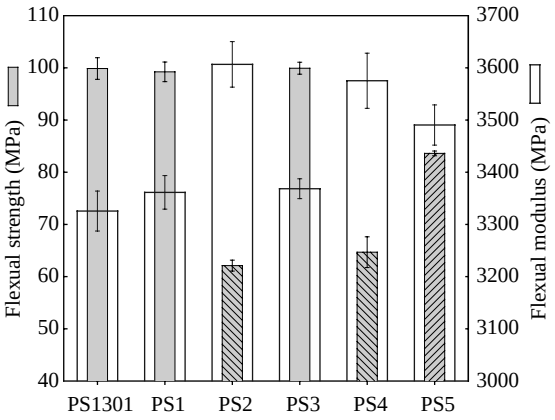

Fig. 11. Flexural strength and modulus of as received PS1301 and its PNC's with COPS or C10A compounded in TSE-34 or TSE-34+GP+EFM (gap= 15 μm).

Since the partially crosslinked COPS domains are expected to be deformable, the apparent dynamic yield stress should follow the dependence derived for immiscible polymer blends [23]:

$$\sigma_y(\omega) = \sigma_y^0[1 - \exp\{-\tau_y\omega\}]^u \quad (2)$$

where σ_y^0 is the apparent yield stress, τ_y is the relaxation time of the domain-to-domain interactions, and $u = 0.2$–1.0 is an exponent dependent on the polydispersity of drop (or aggregate) size. Combining Eq. (2) with Eq. (1) provides means for extracting the dynamic yield stress from η' vs. ω plot (in these calculation $u = 1$ was assumed).

As evident from data in Fig. 6(b), Eqs. (1) and (2) well describe the observed dependencies. The equation parameters extracted from the fitting, η_0 and σ_y, are listed in Table 1, and plotted vs. composition in Figs. 13 and 14, respectively.

The relative viscosity in Fig. 13 was described using Simha's equation [24]:

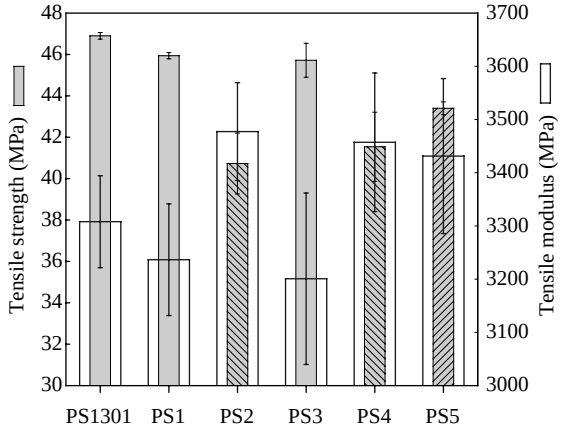

Fig. 10. Tensile strength and modulus of as received PS1301 and its PNC's with COPS or C10A, prepared in TSE-34 or TSE-34+GP+EFM (gap=15 μm).

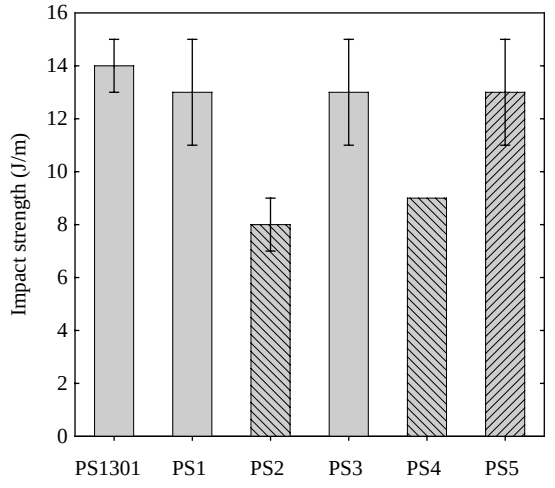

Fig. 12. Impact strength of as received PS1301 and its PNC's with COPS or C10A compounded in TSE-34 or TSE-34+GP+EFM (gap=15 μm).

Table 2
Parameters of the generalized Carreau–Yasuda equation: as determined for PS1301 and its mixtures with C10A and COPS at 180 °C (Table 1)

Parameters	PS1303 as received	PS3 (PS1301)	PS4 (PS1301/COPS)	PS5 (PS1301/C10A)	PS20.3 at $T=160$ °C
r^2	0.99997	0.99996	0.99993	0.99995	0.99997
η_0 (kPa s)	76.60±0.45	55.04±0.20	45.72±0.17	64.95±0.56	77.65±0.11
τ (s)	2.06±0.13	1.56±0.06	1.14±0.06	1.71±0.21	3.0±0.04
n	0.001±0.017	0.012±0.011	0.007±0.015	0.027±0.036	0.209±0.003
a	0.624±0.009	0.639±0.006	0.634±0.008	0.652±0.018	0.813±0.004

Note: r^2 is the correlation coefficient squared; the other parameters are those of the generalized Carreau–Yasuda equation.

$$\eta_r = \frac{1 + 4[\eta]\phi(1-y^7)}{4(1+y^{10}) - 25y^3(1+y^4) + 42y^5} \tag{3}$$

$$y = \left[2\left(\frac{1}{\tilde{\phi}}\right)^{1/3} - 1\right]^{-1}; \quad \tilde{\phi} \equiv \frac{\phi}{\phi_m}$$

Eq. (3) was derived for suspensions of hard spheres and it has two parameters, the intrinsic viscosity, $[\eta]$ (which for hard spheres equals 5/2), and the maximum packing volume fraction, ϕ_m. For suspensions of solid particles the values of these parameters depend on the particle shape and aspect ratio [25]. For the data displayed in Fig. 13 a non-linear least squares fitting gave the following values: $[\eta]=76.74\pm37.46$, and ϕ_m 0.115 ± 0.035. Assuming disk-like particles, their aspect ratio may be calculated from $[\eta]$ and ϕ_m as: $p=230\pm80$, and 120 ± 86, respectively. Since the aspect ratio of a single MMT platelet is about 300, the smaller values calculated from the flow behavior indicate presence of stacks. According to XRD in Part I, an approximate value of the interlayer spacing for COPS in PS20.3 is $d_{001}=7.9$ nm, thus according to the dynamic flow behavior the number of clay platelets per stack should be ca. 2–3, which is comparable with an average XRD value of about 3.

Fig. 14 shows the concentration dependence of four rheological parameters for PS20.3 with 0, 12.5, 25, and 50-wt% COPS, determined at $T=160$ °C and $\gamma_0=0.05$. The graph was constructed by first plotting the apparent yield stress, $\sigma_y=\sigma_y^o$, and its linear fit. Extrapolating the latter to zero determined the critical COPS concentration, $w_c=8.9$-wt% (marked by the vertical line), at which the onset of yield stress is expected. Next, the other rheological functions were placed on the figure: the initial slopes of dynamic and loss shear moduli, $d\ln G'/d\ln\omega$, $d\ln G''/d\ln\omega$, and the crossover frequency at which the moduli are equal, $\omega_x=\omega|_{(G'=G'')}$. As shown in Fig. 14, $\omega_c=8.9$-wt% is indeed a boundary concentration for rheological behavior, i.e. at this concentration the PS/COPS system becomes unduly elastic.

The term 'unduly' is to indicate that such a behavior would not be expected from a single-phase, homogenous melt. Its origin is the presence of interacting soft gel domains. Were the domain made off monodispersed hard spheres, the onset of interaction would be expected at the percolation threshold, $\phi_{perc}=0.156$, not at $\phi_{COPS}=0.054$. Considering that on the one hand COPS contains a soluble portion in PS and on the other that the size of the domains is polydispersed, the effective volume fraction of the soft gel domains at the onset of interaction is expected to be significantly smaller than that.

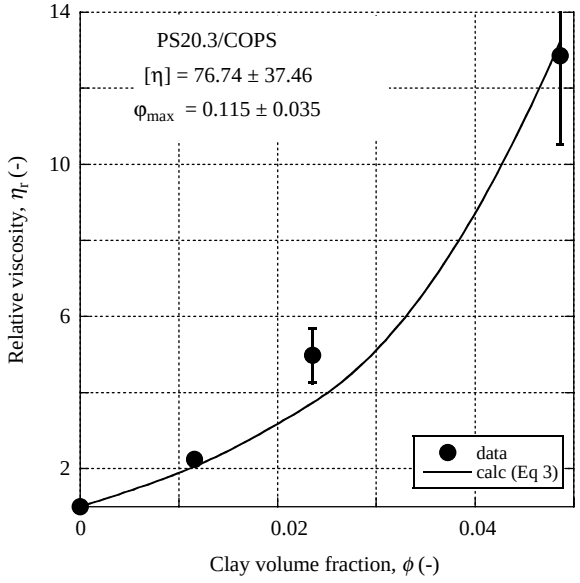

Fig. 13. Relative zero-shear viscosity of the PS20.3 with 0, 12.5, 25, and 50-wt% COPS vs. MMT volume fraction.

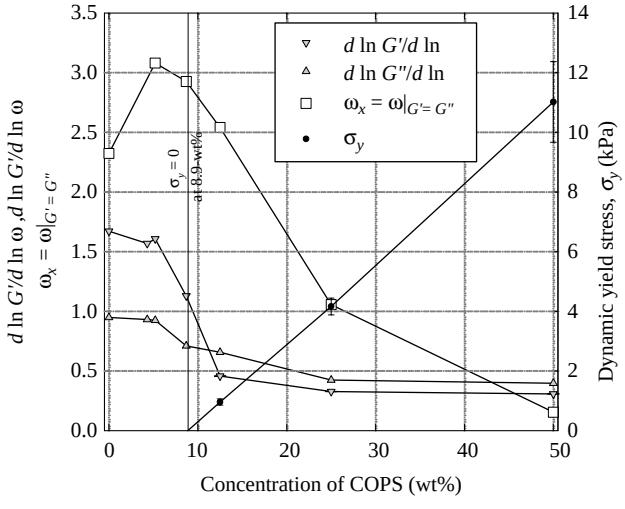

Fig. 14. Concentration dependence of the rheological parameters (initial slopes of dynamic and loss moduli, the crossover frequency at which the moduli are equal and the dynamic yield stress) for PS20.3 with 0, 12.5, 25, and 50-wt% COPS. See text.

Since the percolation threshold depends on the aspect ratio [26] the small value indicates a departure from spherical symmetry. For particles with large aspect ratio, p, the relation between ϕ_{perc} and p is [27,28]:

$$\frac{1}{\phi_{perc}} = a_0 + a_1 p; \quad \text{or} \quad p\phi_{perc} \approx \text{const} \tag{4}$$

where a_0 and a_1 are parameters. For disks the values: $a_0 = 0.514$ and $a_1 = 0.872$ were calculated from the published results [29]. Since for the interacting COPS aggregates ϕ_{perc} is at least three times smaller than that for hard spheres, their aspect ratio is: $p(\text{aggregate}) > 3$. To get a more precise estimate one may use Padé-type approximation [30], valid in the full range of aspect ratios. These calculations give $p(\text{aggregate}) > 8$. It might be expected that in a stationary melt the soft aggregates adopt a spherical symmetry. The value of $p > 8$ suggests flattening by shear at the starting high frequency, $\omega = 100$ rad/s. The oblate shape persists as the frequency decreases (note that the relaxation time of a single clay platelet was determined as ca. 3600 s [31]).

Fig. 7 displays the relationships between G' and G'' for PS1301 with ca. 1.2-wt% MMT (introduced by incorporating either 5.2-wt% COPS or 2-wt% C10A) and also for PS20.3 containing 0, 12.5, 25, and 50-wt% COPS (samples B21 and B23 to B25). As evident from Fig. 7(a), at low frequencies all dependencies follow the power-law dependence: $G' \propto G''^{1.7}$. At high frequencies, $\omega > 10$ rad/s, the dependencies for PS1301 and the two PNC's are quite different—the reason for this diversity is unknown. It is worth recalling that the Doi and Edwards model gives:

$$\log G' = 2\log G'' + \log\left(\frac{6M_c}{5\rho RT}\right) \tag{5}$$

where M_c is the molecular weight between cross-links, ρ the density, R the gas constant and T the temperature. Thus, the power-law exponent 2, not 1.7, is expected.

Evidently, there is a significant difference of behavior with that presented in Fig. 7(a)—while incorporation of 5.2-wt% of COPS (i.e. 1.13-wt% MMT) did not change the character of the G' vs. G'' dependence, an increase of COPS content to $\geq$12.5-wt% (MMT content $>$2.7-wt%) strongly affected it. The presence of COPS unduly increased the system elasticity at the same level of the viscous loss. For PNC's with 12.5 and 25-wt% the systems remain mostly within the domain of the linear viscoelastic behavior, whereas for 50-wt% a non-linear viscoelasticity is observed.

4.2. Viscoelastic behavior of PS/COPS

Owing to the effective network structure of COPS, attempts to measure its melt rheological behavior have failed. In the parallel plates tooling the specimens looked crumbly and unmelted, the temperature inside the specimen was non-homogeneous, and attempts to impose dynamic shearing resulted in irreproducible wall slip. As discussed above, incorporation of 25-wt% COPS into PS matrix caused viscoelastic non-linearity at higher frequencies, which dominated the dynamic moduli at 50-wt% COPS loading. The latter composition was the highest at which the dynamic melt rheometry could be applied.

To study the viscoelastic behavior of neat COPS, the DMTA measurements were carried out using its mixtures with PS20.3 in the full range of concentration from 0 to 100-wt%. The results are presented in Figs. 8 and 9.

Fig. 8 displays the tensile dynamic storage and loss moduli, E' and E'' at $T = 30$–170 °C, i.e. on both sides of the glass transition temperature, T_g (taken as the temperature at which E'' reaches maximum). At low temperatures ($T < T_g$) the moduli of the five specimens separate into two categories, one for COPS $\leq$12.5-wt% and the other for higher COPS concentrations. At high temperatures ($T > T_g$), E' and E'' of neat COPS show a secondary plateaux, similar to what has been observed for crosslinked systems [32].

Fig. 9 displays master curves of E' and E'' as functions of reduced frequency, ωa_T. The plot spanning 19 decades of deformation rate was generated applying the time–temperature (t–T) superposition principle to data obtained during low strain ($\gamma = 0.0004$) frequency sweeps, from $\omega = 0.0628$ to 62.8 rad/s, at $T = 30$–170 °C, with the step of $\Delta T = 10$ °C. The master curves were obtained for PS20.3, PS/COPS 50/50, and COPS.

For a single-component system, the horizontal, a_T, and vertical, b_T, t–T shift factors are expressed as [33]:

$$a_T = \left(\frac{(\eta_0/\rho T)_T}{(\eta_0/\rho T)_{T_{ref}}}\right); \quad b_T = \frac{(\rho T)_{T_{ref}}}{(\rho T)_T} \tag{6}$$

$$\therefore a_T = \frac{b_T \eta_0}{(\eta_0)_{T_{ref}}}$$

where ρ is density, T is temperature and T_{ref} is the reference temperature. The vertical shift factor, b_T, corrects for the volume expansion with temperature, whereas the horizontal shift factor, a_T, for the volume as well as zero shear viscosity.

Similarly as in Fig. 8, at high frequencies (i.e. low temperatures, $T < T_g$) E' of specimens containing COPS $\geq$50-wt% superpose, while that of PS is significantly lower. The peak of loss modulus (T_g) of PS is narrowest, broadening for 50, than more for 100-wt% COPS.

At high temperatures ($T > T_g$) E' of neat COPS show a small secondary peak, similar to what has been observed for the crosslinked systems. The peak is more evident on the E'' master-curve, at $\log(\omega a_T) = -10$ (at $\omega = 6.28$ rad/s equivalent to $T > 181$ °C, or over 80 °C above T_g of PS). Within this range of the reduced frequency, the storage and loss moduli of COPS are higher by about one decade than these of PS20.3. Considering that E'' peaks indicate transitions, the secondary one may originate in the breakup of the ammonium ion pairs or clusters [34].

The temperature dependencies of the shift factor, a_T, for PS with 0, 50, and 100-wt% of COPS (obtained from t–T superposition) are displayed in Fig. 15. Near the glass transition temperature, $T_g < T(°C) < T_g + 100$, the temperature dependence of a_T for polymer melts follows the

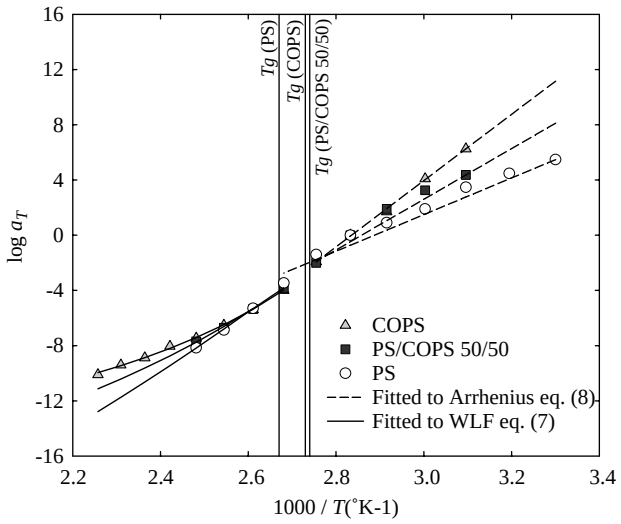

Fig. 15. Temperature shift factor, a_T, as a function of $1/T$ for PS with 0, 50, and 100-wt% of COPS. The glass transition temperatures for PS20.3 neat COPS, and 50:50 PS/COPS mixture are indicated.

Williams–Landel–Ferry (WLF) equation:

$$\ln a_T = \frac{-c_1(T-T_0)}{c_2+(T-T_0)} \simeq \frac{-8.86(T-T_g-50)}{101.6+(T-T_g-50)} \quad (7)$$

where T_0 is a reference temperature and c_1 and c_2 are the materials constants [33]. For high temperature melts, as well as for the glassy state, the Arrhenius equation may be used:

$$\ln a_T = \ln A + \frac{E_a}{RT} \quad (8)$$

where A is pre-exponential factor, E_a is the activation energy, and $R=8.31432$ J/mol K is the universal gas constant.

The a_T data for PS20.3 with 0, 50, and 100-wt% COPS belong to two different dynamic regions, divided by the glass transition temperature, T_g. Within the glassy region ($T<T_g$) the segmental motion is restricted, activated by T, and the dependence should follow the Arrhenius Equation (8). By contrast, at $T>T_g$, the motion (dependent on the free volume) should follow WLF dependence, Eq. (7); only at $T>T_g+100$ the T-activated motion is expected [33]. Results of these calculations are shown in Fig. 15, with the equation parameters listed in Table 3.

4.3. Mechanical performance

Since a large amount of material is needed to prepare specimens for the mechanical tests, only samples prepared in TSE-34 or TSE+GP+EFM (specimens PS1 to PS5 in Table 1) were examined. The injection-molded specimens were tested for the tensile, flexural, and impact properties (Figs. 10–12, respectively).

To maximize chances for clay exfoliation, and make clay's effect on performance more evident, the samples PS4 (PS/COPS) and PS5 (PS/C10A) contain low, and similar amounts of MMT—1.13 and 1.22-wt%, respectively. For the same reason the highly efficient compounding line of TSE+GP+EFM was used. For comparison, the results of 'as received' PS, the same resin extruded in TSE-34, and that in TSE+GP+EFM are also shown. The relative merit of compounding, as well as that of clay incorporation is summarized in Table 4, where the difference (in %) between Y-property of the 'specimen' in column 1 and that of the 'reference' in column 2 is given:

$$\Delta(\%) = 100\left(\frac{Y_{\text{specimen}}}{Y_{\text{reference}}}-1\right)$$

The average error of these measurements are shown in Figs. 10–12, as well as in Table 4.

Thus, extrusion of PS1301 in the TSE alone or in the TSE+GP+EFM (marked as EFM) reduced the tensile strength, tensile modulus and impact strength by 2–2.5, 2.2–3.2 and 7.1%, respectively, i.e. within the error limits of these measurements. However, extrusion of PS1301 with 5.2-wt% COPS in TSE alone resulted in significant reduction of strength (by 11.3, 37.4, and 38.5% for tensile, flexural and impact strength, respectively) accompanied by improved modulus in tensile and flexural test by ca. 7.3%. When the same composition was extruded in TSE+GP+EFM the reduction of strength was severe, while the moduli remained similar to those obtained using TSE alone. Finally, replacing COPS by C10A, and extruding the mixture in TSE+GP+EFM resulted in PNC with the smallest reduction of strengths, and slightly improved stiffness.

For the best exfoliated PNC's, the relative modulus, $E_R = E_{CPNC}/E_{matrix}$, increases with clay content, w, following an empirical dependence [1]:

$$E_R \equiv \frac{E_c}{E_m} \cong 1+0.2w$$

Table 3
Fitting parameters of Eqs. (7) and (8) for a_T vs. T data displayed in Fig. 15

Sample	T_g (°K)	Applied at	Eq.	A	E_a (kJ/mol)	T_0[a] (°K)	c_1	c_2 (°K)	r^2
COPS	365.75	$T\leq T_g$	(8)	$\cong 0$	459.52	–	–	–	0.999
		$T>T_g$	(7)	–	–	353.15	42.74	210.8	0.998
PS/COPS 50/50 (B25)	363.95	$T\leq T_g$	(8)	$\cong 0$	351.46	–	–	–	0.995
		$T>T_g$	(7)	–	–	353.15	24.33	106.7	0.993
PS (B21)	375.15	$T\leq T_g$	(8)	$\cong 0$	254.17	–	–	–	0.995
		$T>T_g$	(7)	–	–	353.15	17.33	66.6	0.968

[a] Chosen temperature

Table 4
Summary of mechanical modification (Δ%) of the samples prepared in TSE-34 or in TSE-34+GP+EFM (gap=15 μm)

Specimen	Reference	Δ Tensile strength	Δ Tensile modulus	Δ Flexural strength	Δ Flexural modulus	Δ Impact strength
Error of measurements (%)	1.8	3.6	2.0	1.1	11.0	
PS (TSE)	PS (as received)	−2.0	−2.2	−0.6	1.1	−7.1
PS (EFM)	PS (as received)	−2.5	−3.2	0.1	1.3	−7.1
PS/COPS (TSE)	PS (TSE)	−11.3	7.4	−37.4	7.3	−38.5
PS/COPS (EFM)	PS (EFM)	−9.1	8.0	−35.3	6.1	−30.8
PS/C10A (EFM)	PS (EFM)	−5.1	7.2	−16.3	3.6	0

Thus, for PS4 and PS5 (containing 1.13 and 1.22 MMT, respectively) the expected enhancement of the PS Young's modulus is by 26 and 44%, respectively. Evidently, the obtained values are much smaller.

The results of XRD, SEM and rheological measurements indicate that PS4 containing 5.2-wt% COPS has a two-phase structure: PS matrix and dispersed in it large, easily deformable domains of partially crosslinked MMT-PS-*co*-VBTA copolymer. Within the COPS domains the clay interlayer spacing is relatively large (d_{001}=7–8 nm), and so is the number of clay platelets per statistical stack, m=3–12. Thus, the clay reinforcing effect is restricted to the dispersed domains. However, since the surface energy of crystalline solids is unusually high, the intercalating co-polymer is adsorbed onto clay surface as a low mobility layer. The thickness of the adsorbed polymer layer was reported [35] to be about 6 nm, i.e. the stacks act as partially solid, low aspect ratio bodies, having low reinforcing effect.

The data in Table 4 indicate that addition of COPS to PS has a detrimental effect on strength. There are several possible sources of this effect: a modest stiffening of the system (which may reduce toughness), COPS immiscibility, and the plasticating effect of extractable from COPS low molecular weight compound, viz. styrene, oligostyrene, etc.

The PS-based PNC's prepared with Cloisite® 10A shows notoriously poor performance [6–9,36]. Three reasons have been identified: small interlayer spacing (d_{001}=3–4 nm), immiscibility of the 2MBHTA intercalant with PS matrix, and poor thermal stability of C10A, which during compounding causes a collapse of clay stacks. In this work incorporation of C10A (see PS5) slightly improved PS stiffness. However, its effect on strength was relatively mild. It seems that in spite of immiscibility, the dispersed short stacks of C10A (m=3–4) have smaller strength reducing effect than the large COPS domains. In the final account, the overall performance of PS5 was comparable (there is a small difference in MMT content), or slightly better than that of PS4.

5. Conclusions

The main objective of this work was to prepare exfoliated PNC with PS as the matrix. For this purpose, COPS organoclay with macromolecular intercalant was synthesized, and then melt-compounded with PS. The clay platelets in COPS and its PNC with PS, have the interlayer spacings of d_{001}=7–8 nm, but the number of clay platelets per stack is unusually large: m=3–12. The scanning and transmission electron microscopy indicated that in PS matrix COPS formed large, immiscible domains.

The rheological behavior in the molten and glassy states was studied. Since the time sweeps indicated the presence of volatiles in materials containing COPS (which caused increases of G' and G'' during the rheological tests) the rheological data were corrected, extrapolating to zero-test time. Two sets of frequency scans were obtained, the first for PS and PNC containing low concentration of MMT, viz. ca. 1.2-wt%, and the second contained ≥2.7-wt% MMT.

For the first set good superposition of G' vs. G'' indicated common melt structure and linear viscoelastic behavior. However, while incorporation of 2-wt% C10A into PS increased the zero-shear viscosity by ca. 20%, that of 5.2-wt% COPS (containing about the same amount of MMT) reduced it by ca. 18%. The reduction most likely is caused by the presence in COPS of extractable oligomers.

Dramatically different rheological behavior was observed for the second set. Here, the relation between G' and G'' indicated that addition of 12.5-wt% COPS (2.71-wt% MMT) unduly increased the system elasticity at the same level of the viscous loss. For PNC's with 12.5 and 25-wt% COPS the systems remain mostly within the linear viscoelastic region, whereas for 50-wt% a non-linear viscoelasticity was observed. In short, the second set behaved as a partially crosslinked system, with the crosslinking density increasing with COPS content.

To define the critical overlap concentration, w_c, at which the behavior of set one is transformed into that of set two, two rheological functions were used, namely the dynamic yield stress, and the cross-over frequency at which the moduli are equal, $\omega_x=\omega|_{(G'=G'')}$. These dependencies consistently indicated that w_c=5.8-wt% of COPS. More detailed analysis of the PNC structure during flow suggested that COPS stacks are distorted by the dynamic shear, becoming elongated, with the apparent aspect ratio of COPS domains >8.

The viscoelastic behavior of neat COPS and PNC's was studied by DMTA from T=30–170 °C, i.e. on both sides of the glass transition temperature, T_g. At low temperatures ($T<T_g$) the moduli of specimens containing ≤12.5-wt% COPS showed similar behavior, but different than those observed for higher COPS concentrations. At high temperatures ($T>T_g$), E' and E'' of neat COPS show a secondary plateaux, similar to what has been observed for crosslinked systems. Furthermore, the master curves of E' and E'' were constructed as functions of 19 decades of reduced frequency. At higher temperatures

($T > T_g$) the moduli of neat COPS showed a small transition peak, at $T > 181$ °C for $\omega = 6.28$ rad/s. The transition may originate in the breakup of the ammonium ion pairs.

The mechanical properties of samples (prepared in a highly efficient compounding line of TSE + GP + EFM with ca. 1.2-wt% MMT) were tested for the tensile, flexural, and impact behavior. For comparison, PS, PS + COPS, and PS + C10A were examined. Both PNC's showed poor performance; stiffness of PS/COPS samples was ca. 18% of what could be expected of homogenous, fully exfoliated PNC, whereas that of PS/C10A was about 27%. Furthermore, addition of COPS resulted in significant reduction of strength in tensile, flexural and impact strength. In short, the overall performance of PS/COPS was slightly inferior to that of PS/C10A.

Acknowledgements

The authors gratefully acknowledge help from the technical staff of the NRCC/IMI, especially that from Chantal Coulombe, Florence Perrin, Yves Simard, and Manon Plourde.

References

[1] Utracki LA. Clay-containing polymeric nanocomposites. 1st ed. Shawbury, Shrewsbury, Shropshire, UK: RAPRA; 2004.
[2] Tokihisa M, Yakemoto K, Sakai T, Utracki LA, Sepehr M, Li J, et al. Proceedings of the PNC-2005 international conference, Boucherville, Que., Canada 2005.
[3] Lim YT, Park OO. Macromol Rapid Commun 2000;21:231.
[4] Lim YT, Park OO. Rheol Acta 2001;40:220.
[5] Wang H, Zeng C, Elekovitch M, Lee LJ, Koelling KW. Polym Eng Sci 2001;41:2036.
[6] Uribe J, Kamal MR, Garcia-Rejon A, Utracki LA. Proceedings of the polymer processing society annual meeting, Guimarães, Portugal 2002.
[7] Tanoue S, Utracki LA, Garcia-Rejon A, Tatibouët J, Cole KC, Kamal MR. Polym Eng Sci 2004;44:1046.
[8] Tanoue S, Utracki LA, Garcia-Rejon A, Kamal MR. Polym Eng Sci 2004; 44:1061.
[9] Tanoue S, Utracki LA, Garcia-Rejon A, Tatibouët J, Kamal MR. Polym Eng Sci 2005;45:827.
[10] Hofmann AW. Justus Liebigs Ann Chem 1851;78:253.
[11] Kooli F, Magusin PCMM. Clay Minerals 2005;40:233.
[12] Balazs AC, Singh C, Zhulina E. Macromolecules 1998;31:8370.
[13] Kim K, Utracki LA, Kamal MR. J Chem Phys 2004;121:10766.
[14] (a) Xu F, Qutubuddin S. Mater Lett 2000;42:12.
(b) Xu F, Qutubuddin S. Polymer 2001;42:807.
[15] Uthirakumar P, Hahn YB, Nahm KS, Lee Y-S. Eur Polym J 2005;41: 1582.
[16] Zhong Y, Zhu Z, Wang S-Q. Polymer 2005;46:3006.
[17] Khalil H, Mahajan D, Rafailovich M. Polym Int 2005;54:423, 428.
[18] Hoffmann B, Dietrich C, Thomann R, Friedrich C, Mülhaupt R. Macromol Rapid Commun 2000;21:57.
[19] Zheng X, Wilkie CA. Polym Degrad Stab 2003;81:539.
[20] Su S-P, Jiang DD, Wilkie CA. Polym Degrad Stab 2004;83:333.
[21] Du J-X, Wang D-Y, Su S, Wilkie CA, Wang J-Q. Polym Degrad Stab 2004;83:29.
[22] Sepehr M, Utracki LA, Zheng X, Wilkie CA. Part I of this paper.
[23] Utracki LA. Polymer alloys and blends. Part 3. Munich: Hanser Publishers; 1989.
[24] Simha R. J Appl Phys 1952;23:1020.
[25] Part 3.3 in Ref. [1].
[26] Katsura T, Kamal MR, Utracki LA. Adv Polym Technol 1985;5:193.
[27] Yi JY, Choi GM. J Electroceram 1999;3:361.
[28] Flahaut E, Peigney A, Laurent C, Marliere C, Chastel F, Rousset A. Acta Mater 2000;48:3803.
[29] Celzard A, McRae E, Deleuze C, Dufort M, Furdin G, Marêché JF. Phys Rev B 1996;53:6209.
[30] Garboczi EJ, Snyder KA, Douglas JF, Thorpe MF. Phys Rev E 1995;52: 819.
[31] Utracki LA, Lyngaae-Jørgensen J. Rheolog Acta 2002;41:394.
[32] McKenna GB. In: Mark H, editor. Encyclopedia of polymer science and technology, 3rd ed, vol. 4. New York: Wiley-Interscience; 2003.
[33] Ferry JD. Viscoelastic properties of polymers. 3rd ed. New York: Wiley; 1980.
[34] Charlier P, Jérôme R, Teyssié P, Utracki LA. Macromolecules 1992;25: 2651.
[35] Luengo G, Schmitt F-J, Hill R, Israelachvili JN. Macromolecules 1997; 30:2482.
[36] (a) Nassar N, Utracki LA, Kamal MR. Int Polym Process 2005. Accepted for publication.
(b) Utracki LA, Sepehr M, Li J. Melt compounding of Polymeric Nanocomposites. Invited paper, Int Polym Process 2005. Accepted for publication.